**HEFAT2010**
**7th International Conference on Heat Transfer, Fluid Mechanics and Thermodynamics**
**19-21 July 2010**
**Antalya, Turkey**

# NUMERICAL EVALUATION OF THE NACA 0012 AIRFOIL DRAG COEFFICIENT EMPLOYING A POLYHEDRAL MESH

Beck, P.A*, Vielmo, H.A. and Petry, A.P.
*Author for correspondence
Mechanical Engineering Department
Federal University of Rio Grande do Sul
Rua Sarmento Leite 425
Porto Alegre, RS, CEP 90050-170
Brazil
E-mail: 00080322@ufrgs.br

## ABSTRACT

The prediction of the aerodynamic drag coefficient of airfoils is essential in the design of wings and blades of wind turbines. The evaluation of the drag coefficient of a NACA 0012 airfoil at zero degrees angle of attack relies on the Finite Volumes Method adopted by the commercial software Star-CD, being the RANS equations solved at selected Reynolds numbers. The discrete domain consists of polyhedral cells, which minimizes the number of faces per unit volume as compared to hexahedral and tetrahedral meshes. The present work investigates the steady state regime for selected Reynolds numbers, comparing the results to the experimental ones available in literature. The airflow is incompressible over the airfoil's adiabatic walls where the non-slip condition is enforced. The molecular viscosity is constant and the turbulence model adopted is the k-omega/SST/Low Reynolds with hybrid wall function. The calculation of the flow field runs the SIMPLE algorithm. The differencing schemes are LUD for momenta, UD for kinetic turbulent. Constructive aspects of the polyhedral mesh that influences the computational effort, the choice of the turbulence model and the number of wall cells required to achieve acceptable values for $y^+$ and $c_d$ are presented and discussed.

## INTRODUCTION

The prediction of the aerodynamic drag coefficient of airfoils is of essence in the design of wings and blades of wind turbines for power generation, being the lift-to-drag coefficients ratio ($C_L/C_D$) an important performance parameter (figure of merit) of such applications.

The lift acting on an airfoil can be calculated assuming inviscid flow in conjunction with the Kutta condition at the trailing edge. This same approach yields zero drag when used to predict drag and experimental or numerical methods are therefore in place. Experiments may not completely reproduce the physical model due to interference or measurement difficulties. Numerical methods were limited to potential flow solvers for evaluating the induced drag in attached flow conditions.

Advances in computing performance have led to widespread use of RANS (Reynolds-averaged Navier-Stokes) equations solvers. The error margin of these solutions is an issue [1] and three major aspects that may compromise the results can be outlined: the need to have a very closely spaced grid in the vicinity of the walls in order to obtain suitable numerical values for the velocity gradient at the wall $(\partial u/\partial y)_w$ from which $\tau_w$ (wall shear stress) is obtained; the uncertainty in the accuracy of turbulence models when a turbulent flow is being calculated and the lack of ability of most turbulence models to predict transition from laminar to turbulent flow. The fore mentioned aspects are here approached by investigating the results when a polyhedral mesh is adopted in conjunction with the low Reynolds variant of the k-omega/SST turbulence model [2] with hybrid wall boundary condition.

In order to obtain the lift-to-drag ratio *L/D* for aerodynamic bodies like a finite wing, both $C_L$ (lift coefficient) and $C_D$ (drag coefficient) must be known. The lift distribution is obtained from the Kutta-Joukowski theorem and its integration over the wing's span allows calculating $C_L$. Prandtl's classical lifting line theory [1], ultimately expressed by Eq. (1), may then be used to estimate $C_D$ as follows:

$$C_D = c_d + \frac{C_L^2}{\pi e AR} \tag{1}$$

In Eq. (1), $C_L$ is the lift coefficient, $AR = b^2 / S_{ref}$ is the wing aspect ratio where $b$ is the wing span and $S_{ref}$ a

reference area, "$\pi e$" is the $\pi$ constant multiplied by the Oswald's span efficiency factor "$e$" and $c_d$ is the airfoil drag coefficient per unit span. This article focuses on numerically evaluating $c_d$ for a NACA 0012 airfoil at zero degrees angle of attack for the steady state regime, submitted to subsonic flows. The evaluation relies on the Finite Volumes Method adopted by the commercial software Star-CD, being the RANS equations solved at selected Reynolds numbers. The discrete domain consists of polyhedral and near wall prismatic cells. The results are compared to wind tunnel data available in literature [3].

Constructive aspects of the polyhedral mesh (like the polyhedra growth rate) that influence the computational effort, the choice of the turbulence model and the number of wall cells required to achieve acceptable values for $y^+$ and $c_d$ are presented and discussed here.

## PHYSICAL MODEL AND BOUNDARY CONDITIONS

The physical model is the NACA 0012 airfoil at zero angle of attack. The airfoil's coordinates are given in per cent of the chord and were obtained after computational procedures [4] which have updated and improved in precision the original coordinates values [5].

The ideal gas airflow is treated as incompressible for Mach number $M < 0.3$ over the airfoil's adiabatic and impermeable walls where non-slip condition is imposed. The molecular viscosity $\mu$ = 1.81E-5 Pa.s is constant. The reference density is $\rho_{ref}$ = 1.205 kg/m$^3$ and the reference temperature is $T_{ref}$ = 288 K.

The model's domain is built around the airfoil's geometry as a rectangular box of 0.1 m width, extending 1.8 m upstream the leading edge and 3.6 m downstream the trailing edge. The domain's upper (N) and lower (S) faces are located at 2.28 m each from the airfoil's chord line. The airfoil's chord, 0.6 m, and the model's height-to-chord ratio ($h/c$), 7.6, have been chosen in order to keep the simulated Reynolds and Mach numbers within the range of the "Group 1" summary of wind tunnel test results [3], where the $h/c$ values ranged from 1.9 to 15. The distance from the airfoil's leading and trailing edges to the bounding walls, three and six times respectively the airfoil's chord length, were determined after preliminary trials in such a way that the $c_d$ results became independent of the clearance between the model's edges and its boundaries. Although the $h/c$ value used followed wind tunnel settings, the choice of the model's domain dimensions aimed to mimic free stream conditions and to compare the numerical results to the ones obtained in wind tunnel experiments.

Boundary conditions are required for all the conservation equations. The airfoil's walls are adiabatic where the non-slip and impermeability conditions are imposed. The airfoil's containing box has its upper, lower and side faces set as symmetry planes in order to simulate the free stream conditions applied to an infinite wing, therefore turning the numerical model bi-dimensional as the wind tunnel settings [3]. The front face is the model's inlet region where velocity is prescribed in accordance to the Reynolds number at the airfoil's chord as presented in Tab. 1. The piezometric pressure boundary condition is applied on the rear face and referenced to the atmospheric pressure of 101325 Pa.

**Table 1**. Boundary conditions at the inlet region.

| *U (m/s)* | *M* | *Re* |
|---|---|---|
| 25,03 | 0,07 | 1,0E+06 |
| 50,07 | 0,15 | 2,0E+06 |
| 75,10 | 0,22 | 3,0E+06 |

The turbulence mixing length of the airflow at the inlet region, 1E-3 m, is set to an order of magnitude smaller than the turbulent boundary layer thickness at the trailing edge of a flat plate of length 0.6 m and Reynolds number $Re$=3E6, calculated as 1.12E-2 m. The turbulence intensity was set very low (1E-4) in order to simulate experimental wind tunnel inlet conditions and to minimize the changes in the pressure and shear distributions over the airfoil's walls that could influence the airfoil's drag coefficient value [6]. At the pressure boundary, the values for the turbulence parameters are calculated by the code on the assumption of zero gradients along the streamlines intersecting the boundary surface. Figure 1 depicts the physical model and its polyhedral mesh.

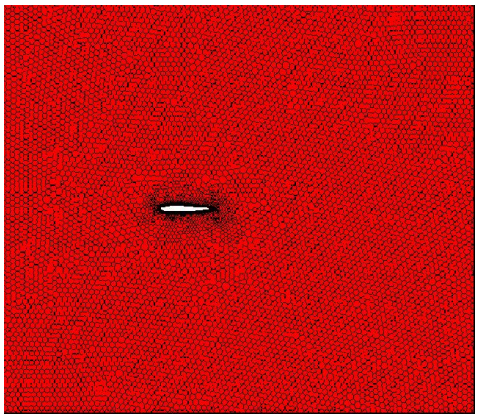

**Figure 1.** The physical model and the polyhedral mesh.

## MATHEMATICAL MODEL

The governing equations describing the airflow over the airfoil's walls are the Navier-Stokes equations and the closure equations corresponding to the turbulence model.

All the equations are solved concurrently and the pressure-velocity coupling is made by the SIMPLE algorithm [7].

The mass and momentum equations are, in Cartesian notation [8], Eq. (2) and Eq. (3) respectively:

$$\frac{\partial \rho}{\partial t} + \frac{\partial}{\partial x_j}(\rho u_j) = s_m \tag{2}$$

$$\frac{\partial \rho u_i}{\partial t} + \frac{\partial}{\partial x_j}(\rho u_j u_i - \tau_{ij}) = -\frac{\partial p}{\partial x_i} + s_i \tag{3}$$

In the equations above, $t$ is a time variable, $x_i$ a cartesian coordinate and $p$ the piezometric pressure.

For turbulent flows, $u_i$, $p$ and other dependant variables, including $\tau_{ij}$ , assume their ensemble averaged values giving Eq. (4)

$$\tau_{ij} = 2\mu s_{ij} - \frac{2}{3}\mu\frac{\partial u_k}{\partial x_k}\delta_{ij} - \overline{\rho u'_i u'_j} \tag{4}$$

In Eq. (4), μ is the molecular viscosity and $\delta_{ij}$ the Kronecker's delta. The $u'$ fluctuations about the ensemble velocity and the over bar denote the ensemble averaging process. The rightmost term in Eq. (4) represents the additional Reynolds stresses due to the turbulent motion. These are linked to the mean velocity via the turbulence model.

The k-omega/SST/Low Reynolds turbulence model has been selected as the closure model since it takes into account pressure gradients and therefore provides more accurate results in terms of wall shear forces.

Defining the specific dissipation rate $\omega = \varepsilon / C_\mu k$ (where ε is the turbulence dissipation rate, $k$ is the turbulent kinetic energy and $C_\mu$ is an empirical coefficient), the governing equations for this model are the turbulence kinetic energy equation, Eq. (5), and the specific dissipation rate equation, Eq. (6):

$$\frac{\partial(\rho k)}{\partial t} + \frac{\partial}{\partial x_j}\left[\rho u_j k - \left(\mu + \frac{\mu_t}{\sigma_k^\omega}\right)\frac{\partial k}{\partial x_j}\right] = \mu_t P - \rho\beta^* k\omega + \mu_t P_b \tag{5}$$

$$\frac{\partial(\rho\omega)}{\partial t} + \frac{\partial}{\partial x_j}\left[\rho u_j \omega - \left(\mu + \frac{\mu_t}{\sigma_k^\omega}\right)\frac{\partial \omega}{\partial x_j}\right] = \alpha\frac{\omega}{k}\mu_t P - \rho\beta\omega^2 + \rho S_\omega + C_{\varepsilon 3}\mu_t P_b C_\mu \omega \tag{6}$$

Although turbulence is a three-dimensional phenomenon, the conservation equations above allow considering the effects of turbulence in a time-average sense. In these equations, $\mu_t$ is the calculated turbulent viscosity and the coefficients α, β, β*, $P$, $P_b$, $C_\mu$, $C_{\varepsilon 3}$, $\sigma_k^\omega$ and $S_\omega$ are either empirically defined or calculated for the SST variant of the k-omega turbulence model [2].

The hybrid wall treatment boundary condition was selected since the normalized parameter $y^+$ was unknown and large variations of this value were expected, thus creating uncertainties as to whether a low Reynolds number boundary treatment or a wall function would be appropriate.

The $y^+$ independency of the hybrid wall condition is achieved by Star-CD using either an asymptotic expression valid for $0.1 < y^+ < 100$ or by blending low-Reynolds and high-Reynolds number expressions for shear stress. In this approach [9], the blending factor ζ, given by Eq. (7), is based on a value of $y^+$ estimated using Eq. (8), a fourth-order asymptotic expansion:

$$\zeta = (1 - e^{-y^+ / y_m^+})^2 \tag{7}$$

$$y^+ = u^+ + \frac{1}{E}(e^{\kappa u^+} - 1 - \kappa u^+ - \ldots - \frac{(\kappa u^+)^4}{4!} \tag{8}$$

In Eq. (8), $u^+ = u / u_*$ where the frictional velocity is $u_* = \sqrt{\tau_w / \rho_{ref}}$, κ is the von Karman's constant and $E$ an empirical coefficient.

After performing the simulation, Eq. (9) is used to obtain the drag coefficient $c_d$ (defined as the ratio between the summation of the computed shear and pressure forces and the dynamic pressure):

$$c_d = \frac{\sum \vec{F} \cdot \vec{d}}{\frac{1}{2}\rho_{ref} U^2 S_{ref}} \tag{9}$$

In Eq. (9), ∑ is the summation over cell faces covering the wall area. The total force is given by $\vec{F} = \vec{F}_w + \vec{F}_p$. The shear force is given by $\vec{F}_w = \tau_w S\vec{V} / \left|\vec{V}\right|$. The pressure force is given by $\vec{F}_p = p \cdot S \cdot \vec{n}$. In the previous equations, $S$ is a wall cell face area, $\tau_w$ is the shear stress acting on the cell face and $\vec{V}$ is the velocity component parallel to the wall at the centre of a near wall cell. $\vec{n}$ is the outward pointing unit vector normal to the wall and $p$ the pressure in the cell face, being $\vec{d}$ the unit vector in the direction of airflow. $\rho_{ref}$ is the reference density, $U$ is the free stream velocity and $S_{ref}$ is the reference area, calculated as the product of the airfoil's chord and the model's span.

## NUMERICAL METHODOLOGY

The model's surface triangulation has been performed using Star-CD's pro-STAR/surf module and the unstructured polyhedral mesh was generated by Star-CD's Automesh feature.

Different triangle length scales ("TLS") were applied to the model's fluid and wall cells in order to achieve several cell densities for grid resolution studies. Typical values for TLS ranged from 80 to 60 mm for the fluid domain and from 6 to 1 mm for the airfoil's walls (approximately 1/200$^{th}$ of the model's characteristic length, i.e., the airfoil's chord). The triangle growth rate was set to 10% at the walls and 20% for the fluid domain.

The polyhedral meshing process requires several parameters to be observed, namely the volume growth rate (set to 1.0), the volume mesh density (also set to 1.0) and the prismatic layer settings. The former ones control the expansion rate and the number of volumes generated by the meshing process, while the number of near-wall volumes is

controlled by the wall's number of triangles. The symmetry between the numbers of volumes generated above and bellows the airfoil's chord line and away from the walls could not be controlled. Prismatic layers were required in order to control the $y^+$ values at the near wall region. Following Star-CD's User's Guide recommendation [10], 20 prismatic layers were used. The stretch factor, defined as the ratio of a prismatic layer thickness to its neighboring (nearer to the wall) layer thickness, was set to 1.2. The total prism layer thickness, 6 mm, produced acceptable $y^+$ values and was selected after preliminary computations. In Fig. 2, the prismatic layers are visible adjacent to the airfoil's walls. Figure 3 presents a close-up view of the model near the airfoil's leading edge.

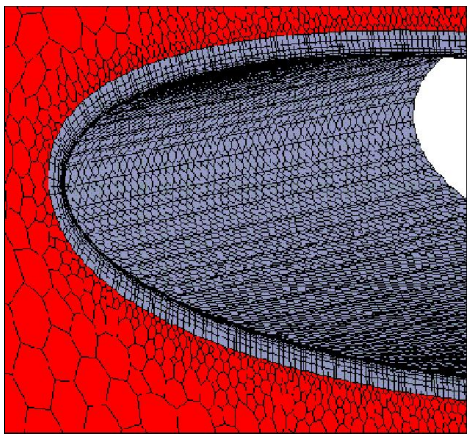

**Figure 2.** The polyhedral mesh and the prismatic layers.

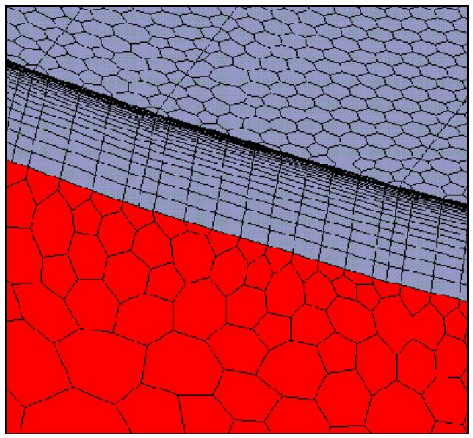

**Figure 3.** Close up view of the near wall region

Grid resolution studies were carried out at Reynolds number 3E6 in order to determine the mesh polyhedra density and the number of wall cells required to achieve converged results for $c_d$. A large number of wall cells were needed in order to be reached the grid independency of the drag coefficient $c_d$ once $y^+$ values stabilize within the turbulence model's limits. The number of wall cells is approximately the same for all Reynolds numbers [11]. Table 2 summarizes the results of the grid resolution studies and shows that over 40.000 wall cells were required to achieve stable values for $c_d$. The $y^+$ values, surface averaged, were kept near 3 at the walls, triggering the low Reynolds wall boundary treatment of the k-omega/SST/Low Reynolds model. The maximum residual value is 1E-5 for mass, momentum and turbulent kinetic energy.

**Table 2.** Grid resolution test results.

| Model No. | Total cells | Wall cells | Re | *cd* | *y+* (wall) |
|---|---|---|---|---|---|
| 1 | 140.507 | 5.936 | 3,0E+06 | 0,0110217 | 2,69 |
| 2 | 165.401 | 7.100 | 3,0E+06 | 0,0110835 | 2,70 |
| 3 | 255.671 | 11.133 | 3,0E+06 | 0,0107085 | 2,66 |
| 4 | 344.771 | 15.029 | 3,0E+06 | 0,0105755 | 2,68 |
| 5 | 421.741 | 17.888 | 3,0E+06 | 0,0096047 | 2,70 |
| 6 | 579.430 | 25.106 | 3,0E+06 | 0,0096548 | 2,70 |
| 7 | 949.569 | 41.299 | 3,0E+06 | 0,0095945 | 2,70 |
| 8 | 1.332.290 | 58.017 | 3,0E+06 | 0,0094929 | 2,72 |
| 9 | 2.020.566 | 87.080 | 3,0E+06 | 0,0094288 | 2,73 |

Momentum, pressure, turbulent kinetic energy and omega were under-relaxed by 0.7, 0.3 and 0.7 respectively. The differencing scheme adopted for momentum was the linear upwind (LUD) with blending factor 1, suited for non-structured meshes in accordance to Star-CD's Methodology book [12]. The upwind (UD) differencing scheme was used for the turbulent kinetic energy and omega [13]. All computations were performed in double precision.

The numerical result's uncertainty has been evaluated by applying to the Models No. 7, No. 8 and No. 9 (from Tab. 2) the generalized Richardson's extrapolation method [14]. Eq. (10) is used to estimate an exact solution where $f_1$ and $f_2$ are the finer and the coarser solutions respectively, $r$ is the effective refinement ratio and $p$ is the observed spatial discretization order.

$$f_{exact} \cong f_1 + \frac{f_1 - f_2}{r^p - 1} \tag{10}$$

The effective refinement ratio $r$ is estimated by Eq. (11), where $N_1$ and $N_2$ are the number of grid points in the finest and the coarser meshes respectively and $D$ is the model's dimensionality, i.e., $D = 3$:

$$r_{effective} = \left( \frac{N_1}{N_2} \right)^{1/D} \tag{11}$$

The observed spatial discretization order is obtained by solving Eq. (12) iteratively for $p$:

$$\frac{\varepsilon_{23}}{r_{23}^p - 1} = r_{12}^p \left[ \frac{\varepsilon_{12}}{r_{12}^p - 1} \right] \tag{12}$$

The stencils "1", "2" and "3" refer to the fine (Model No. 9), intermediate (Model No. 8) and coarse (Model No. 7)

grids, respectively. $\varepsilon_{12} = (f_2 - f_1)/f_1$ and $\varepsilon_{23} = (f_3 - f_2)/f_2$ are the relative solution errors.

The extrapolated result's error band is evaluated by the Grid Convergence Index or *GCI* [15]. For the fine grid, the *GCI* is given by Eq. (13):

$$GCI_{12} = F_s \frac{|\varepsilon_{12}|}{r^p - 1} \tag{13}$$

In Eq. (13), the safety factor $F_s = 1.25$ is adopted as recommended for convergence studies with a minimum of three grids [16].

## RESULTS

A critical assessment of wind tunnel results for the NACA 0012 airfoil has been performed correlating a large quantity of experimental results obtained in more than 40 wind tunnels [3]. These results were summarized in four groups where the wind-tunnel characteristics (like the tunnel's aspect ratio), the Reynolds and Mach numbers range, the use of a boundary-layer trip to induce transition to turbulent conditions and the side-walls effects have been used as a measure of the quality and accuracy of those experiments. The "Group 1" set of experiments stands out as having been conducted with the utmost care by nearly eliminating the important sources of wind-tunnel errors. Figure 4 presents the experimental results obtained for "Group 1" and "Group 2" for the drag coefficient $c_d$ at zero angle of attack, plotted against the Reynolds numbers.

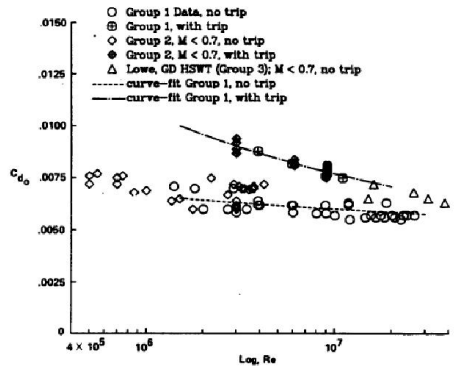


**Figure 4.** Drag coefficient at zero lift vs. Reynolds number. Source: McCroskey, W.J., 1987 [3].

In Fig. (4), the data from Group 1 with a boundary layer trip (crossed circles) and therefore having turbulent airflow over the airfoil's walls is approximated with an overall precision of ± 0.0002 by Eq. (14).

$$c_d = 0.0017 + 0.91/(\log \mathrm{Re})^{2.58} \tag{14}$$

The turbulence mixing length and the turbulence intensity prescribed at the model's inlet region intended to simulate the effect of a physical boundary layer trip which would induce transition to a fully turbulent boundary layer over the airfoil's walls from its leading edge. Preliminary trials using coarser grids showed that the simulated values for the drag coefficient could no longer be influenced by choosing turbulence intensity and length scale values smaller than the ones selected. Therefore, the simulated conditions are closer to the experiments of Group 1 where the boundary layer is fully turbulent and approximated by Eq. (14).

Table 3 compares the numerical results obtained with Star-CD and Model no. 9 (from Tab. 2) to the experimental ones adjusted by Eq. (14). In Tab. 3, the Reynolds numbers ranged from 1E6 to 3E6 (corresponding to free stream Mach numbers $0.07 \geq M \geq 0.22$).

**Table 3.** Numerical results compared to Eq. (14).

| U (m/s) | M | Re | Eq. (14) | k-ω | y+ | Δ% |
|---|---|---|---|---|---|---|
| 25,03 | 0,07 | 1,0E+06 | 0,010642 | 0,011080 | 0,99 | 4,12 |
| 50,07 | 0,15 | 2,0E+06 | 0,009581 | 0,009970 | 1,84 | 4,06 |
| 75,10 | 0,22 | 3,0E+06 | 0,009040 | 0,009429 | 2,73 | 4,31 |

It can be observed from Tab. 3 that the numerical results are nearly 4% higher than the experimental ones [3], where the free stream Mach number ranged from $0.08 \leq M \leq 0.16$ and the Reynolds number calculated at the airfoil's trailing edge varied from 1.4E6 to 3E6 accordingly [17].

In Fig. 5, the values given by Eq. (14) and the numerical results are plotted against the Reynolds numbers.

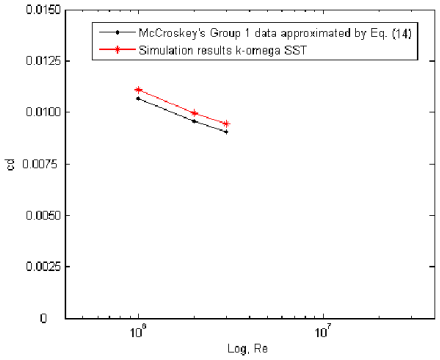


**Figure 5.** Comparison between Eq. (14) and the numerical results vs. Reynolds number.

Table 4 shows that the numerical value obtained with Model No. 9 for $Re$ = 3E6, $f_{exact}$ = 0.0092231, is 2.23 % higher than the extrapolated value obtained for the same model. The extrapolated value's error band, 0.26 %, is given by the $GCI_{12}$ estimate. Also, the observed order of the spatial discretization method is $p$ = 1.95 while the theory predicts $p$ = 2.

The absolute difference between the numerical and the extrapolated value, expressed in terms of drag counts (where one drag count equals 1E-4) is approximately 2. For a subsonic transport aircraft, this difference is equivalent to plus

or minus two passengers [18], a fact that emphasizes the importance of pursuing modelling and numerical accuracy.

**Table 4.** Extrapolated result for Model. No. 9, *Re* = 3E6

| *p* | *r12* | *r23* | *ε23* | *ε12* | *f1* | *f2* | *f3* |
|---|---|---|---|---|---|---|---|
| 1.95 | 1.15 | 1.12 | 0.0107027 | 0.0067983 | 0.0094288 | 0.0094929 | 0.0095945 |

| *f exact* | *GCI12(%)* | *Model #9* | Δ % |
|---|---|---|---|
| 0.0092231 | 0.26480151 | 0.0094288 | 2.23 |

## CONCLUSIONS

The numerical evaluation of an airfoil's drag coefficient can be used as a tool in the process of assessing aerodynamic figures of merit like the lift-to-drag ratio $C_L/C_D$ of finite wings.

Prescribed velocity, pressure and symmetry planes are used as boundary conditions. The airflow is treated as incompressible and the airflow is fully turbulent from the airfoil's leading edge.

The meshing process was performed in two phases – surface triangulation and volume (polyhedra) generation. The number of wall cells is determined by the number of triangles. The number of fluid domain volumes can be modified by changing the volume mesh density and the volume growth rate parameters. A prismatic layer is required in order to keep $y^+$ within limits. The resolution studies showed that grid independence is reached for $c_d$ for a large number of wall cells.

The numerical results for $c_d$ were compared to the experimental results available in literature. In particular, the experiment where the airflow over the airfoil's walls is fully turbulent, the numerical values are approximately 4% higher than the experimental ones.

The extrapolated value for = 3E6, $f_{exact}$ = 0.0092231, has an error band of 0.26 % and the numerical result obtained by simulating Model no. 9 is 2.23% higher than that value.

## REFERENCES


[1] Anderson Jr., J.D., 2007. *Fundamentals of Aerodynamics*. McGraw-Hill.

[2] Menter, F.R.,1993. Zonal two equation k-ω turbulence models for aerodynamic flows. *Proceedings of the 24th Fluid Dynamics Conference*. AIAA Paper 93-2906, pp. 1-21.

[3] McCroskey, W.J., 1987. A Critical Assessment of Wind Tunnel Results for the NACA 0012 Airfoil. *Technical Memorandum 100019*. NASA.

[4] Ladson, C.L., Brooks Jr., C.W., Hill, A.S., Sproles, D.W., 1996. Computer Program To Obtain Ordinates for NACA Airfoils. *Technical Memorandum 4741*. NASA.

[5] Abbott, I.H., von Doenhoff, A.E., 1959. *Theory of Wing Sections*. Dover Publications.

[6] Meier, H.U., Kreplin, H.P., 1980. Influence of Freestream Turbulence on Boundary-Layer Development. *AIAA Journal*, vol. 18, No.1, pp. 11-15.

[7] Patankar, S.V.,1980. *Numeric Heat Transfer and Fluid Flow*. Routledge.

[8] Warsi, Z.V.A.,1981. Conservation form of the Navier-Stokes equations in general nonsteady coordinates. *AIAA Journal*, vol. 19, No.2, pp. 240-242.

[9] Rung, T.,1999. Formulierung Universeller Wandrandbedingungen für Transportgleichungsturbulenzmodelle. *Institutsbericht n.02/99*, Hermann-Föttinger-Institut für Trömungsmechanik, Technische. Universität Berlin.

[10] Star-CD, 2008a. *CCM User Guide*. CD-adapco.

[11] Lombardi, G.,Salvetti, M.V., Pinelli, D.,1999. Numerical Evaluation of Airfoil Friction Drag. *Journal of Aircraft*, Vol. 37, No.2, pp. 354 – 356.

[12] Star-CD, 2008b. *Methodology*. CD-adapco.

[13] Zheng, X., Liu, F., 1995. Staggered Upwind Method for Solving Navier-Stokes and Turbulence Model Equations. *AIAA Journal*, vol. 33, No.6, pp. 991-998.

[14] Roache, P.J., Knupp, P.M., 1993. Completed Richardson Extrapolation, *Communications in Numerical Methods in Engineering*, Vol. 9, pp. 365-374.

[15] Roache, P.J., 1994. Perspective: A Method for Uniform Reporting of Grid Refinement Studies, *ASME Journal of Fluids Engineering*, Vol. 116, pp. 405-413.

[16] Roache, P.J., 1998. *Verification and Validation in Computational Science and Engineering*, Hermosa Publishers.

[17] Gregory, N., O'Reilly, C.L., 1970. Low Speed Aerodynamic Characteristics of NACA 0012 Airfoil Section, Including the Effects of Upper Surface Roughness Simulation Hoarfrost, *NPL Aero Report 1308*, National Physical Laboratory.

[18] Salas, M.D., 2006. Digital Flight: The Last CFD Aeronautical Grand Challenge, *Journal of Scientific Computing*, Vol. 28, No. 213, pp. 479-505.